

🍏PoM: A Linear-Time Replacement for Attention with the Polynomial Mixer

David Picard¹, Nicolas Dufour^{1,2}, Lucas Degeorge^{1,2,4}, Arijit Ghosh¹, Davide Allegro³, Tom Ravaud¹,
Yohann Perron^{1,5}, Corentin Sautier^{1,6}, Zeynep Sonat Baltaci¹, Fei Meng¹, Syrine Kalleli¹, Marta
López-Rauhut¹, Thibaut Loiseau¹, Ségolène Albouy¹, Raphael Baena¹, Elliot Vincent⁷, Loic Landrieu¹

¹LIGM, CNRS, Univ Gustave Eiffel, ENPC, Institut Polytechnique de Paris, France

²LIX, École Polytechnique, CNRS, IP Paris, France ³Department of Information Engineering, Università degli Studi di Padova, Italy

⁴AMIAD, Pole recherche, ⁵EFEO ⁶Valeo.ai, France, ⁷LASTIG, Univ Gustave Eiffel, IGN, Géodata Paris, Paris, France

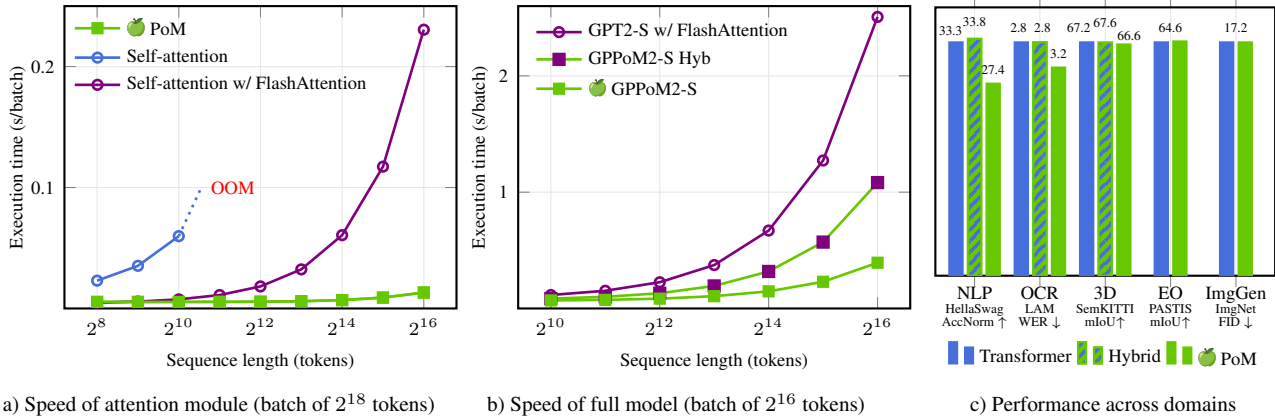


Figure 1. **Polynomial Mixer (PoM)**. Inference time on an H100 as a function of sequence length, shown for the PoM module alone (a) and within a full Transformer pipeline (b). PoM scales nearly linearly and is significantly faster than self-attention for long sequences, even with FlashAttention. As measured for NLP, OCR, 3D point cloud segmentation, Earth Observation analysis, and image generation (c), replacing attention with PoM or hybrid variants preserves accuracy while improving scalability.

Abstract

This paper introduces the Polynomial Mixer (PoM), a novel token mixing mechanism with linear complexity that serves as a drop-in replacement for self-attention. PoM aggregates input tokens into a compact representation through a learned polynomial function, from which each token retrieves contextual information. We prove that PoM satisfies the contextual mapping property, ensuring that transformers equipped with PoM remain universal sequence-to-sequence approximators. We replace standard self-attention with PoM across five diverse domains: text generation, handwritten text recognition, image generation, 3D modeling, and Earth observation. PoM matches the performance of attention-based models while drastically reducing computational cost when working with long sequences. The code is available at <https://github.com/davidpicard/pom>.

1. Introduction

One apple is a supper; one apple is life.

- *Les Misérables, Book Fourth*, Victor Hugo

Multi-Head Attention (MHA) [70] is the key ingredient to recent advances in AI, powering large language models [21, 58, 67], generative models for images and videos [52, 54, 76], as well as breakthroughs in computer vision [20] and speech processing [2, 11, 19, 80]. However, MHA has a quadratic complexity with respect to the input sequence length, severely limiting the attainable context size. Numerous sub-quadratic approximations have been proposed, yet most trade efficiency for either performance or generality. For instance, Linformer [72] requires a fixed sequence length, while State Space Models (SSMs) [55] impose a causal ordering that does not apply to all modalities.

In this paper, we question whether quadratic complexity is truly necessary to match the performance of MHA on sequence-to-sequence tasks. Our approach draws inspiration from the long-standing use of high-order moments

and polynomial features in representation learning [37, 57], which we revisit here as an alternative to attention. We introduce the Polynomial Mixer (PoM), a novel module with linear complexity that achieves comparable performance to MHA across diverse, real-world tasks. PoM aggregates the entire input sequence into a compact representation using a learned polynomial function, computed in linear time. Each token then retrieves relevant contextual information from this summary through a cross-attention-like mechanism.

The *contextual mapping property* [77] is a key aspect of MHA enabling modern transformers to be universal sequence-to-sequence approximators. This property is rarely satisfied by standard neural network components; for instance, MLPs, CNNs, and SSMs do not exhibit it. We show that our proposed Polynomial Mixer (PoM) has the contextual mapping property, allowing it to replace attention blocks in transformers without sacrificing expressivity.

We validate the efficiency and expressivity of PoM across five diverse tasks from different domains: text generation, image generation, optical character recognition, 3D point cloud segmentation, and multi-temporal satellite images analysis. As shown in Fig. 1, PoM matches the performance of MHA while providing a significant speedup on long sequences. Our main contributions are:

- We propose PoM, a token mixing mechanism with linear complexity in the number of tokens.
- We prove that PoM satisfies the contextual mapping property, ensuring transformers equipped with PoM remain universal sequence-to-sequence approximators.
- We demonstrate that PoM achieves performance on par with MHA across five distinct domains, while being substantially more efficient.

2. Related Work

We review prior work on efficient attention mechanisms and alternative architectures that aim to replace or bypass self-attention.

Faster Attention. Since the introduction of Transformers [70], many efforts have been made to reduce the quadratic complexity of MHA [10, 43, 72]. Notably, methods like Reformer [43] use fast approximate neighbors to reduce the size of the attention matrix based on the assumption that most tokens will have zero attention. To go further, Linformer [72] proposes to compute an explicit low rank projection of the keys and the values to reduce the complexity of MHA from the size of the sequence n to an arbitrary chosen number $k \ll n$. The main drawback of such approach is that n and k are fixed, which means that the model can no longer process sequences of varying length. With the advent of Large Language Models and their ability to process extremely long sequences [1, 21, 66], recent efforts have been put on more efficient implementations such

as Flash-Attention [15, 17] or KV-cache [6, 51] which seem sufficient for text. However for visual content, the sequence length grows quadratically with the resolution. Because MHA is also quadratic in the number of tokens, this leads to quartic computational and memory complexity.

Alternatives to Attention. Alternatively, some attempts have been made to remove the Multi-Head Attention entirely, such as in MLP-Mixer [68] and ResMLP [69] that replace MHA with simple projection on the transpose tensor (*i.e.*, considering the sequence dimension as features). These approaches have been shown to obtain competitive results, but similarly to Linformer, they imply a fix sequence length since this length is now an intrinsic dimension of the projection in the transpose direction. More recently, State-Space Models (SSM) [27, 28] have become the focus of recent work especially in language modeling [16, 25, 46, 84]. SSM are recurrent models, which is highly beneficial for language modeling because of the causal property of text: the complexity to generate the next token becomes constant.

In visual content however, there is no such natural causality pattern in the spatial dimensions. Attempt to use such models for vision tasks have been successful [49, 55, 83], albeit at the cost of enforcing an arbitrary 1-dimensional scan order of the tokens that does not encode well the 2D nature of an image. In image generation with diffusion [35, 75], since the model has to be iterated, this results in a doubly sequential processing (space and iterations) that does not benefit from the parallel nature of processing images. For video however, the causal aspect is natural over the time dimension, recurrent approaches may be more efficient. Overall, we question whether a linear time algorithm can achieve the performances of the quadratic attention without imposing causal constraints as SSMs or a fixed sequenced size as Linformer or ResMLP.

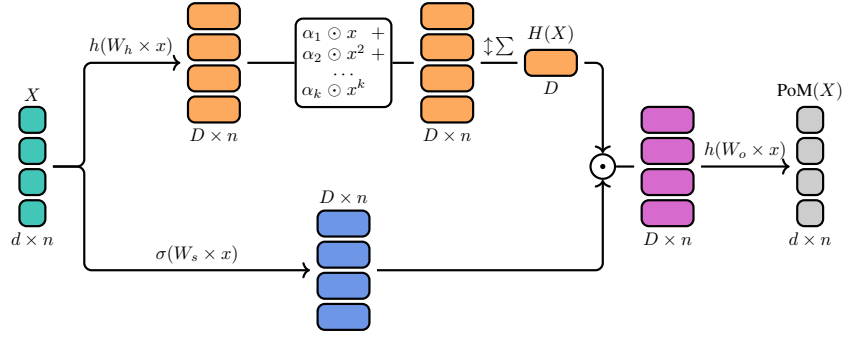
3. Method

In this section, we first describe PoM, our proposed sequence-to-sequence drop-in replacement for MHA (Sec. 3.1). We then propose an extension to causal sequences (Sec. 3.2) and a theoretical analysis (Sec. 3.3)

3.1. Polynomial Mixer and Polymorpher

Polynomial Mixer. We consider an input sequence of n tokens of dimension d , stored in a tensor $X \in \mathbb{R}^{d \times n}$. Unlike MHA, which computes all pairwise interactions between tokens, the Polynomial Mixer relies on a shared *state representation* $H(X)$ that serves as a common memory accessible to all tokens. This state aggregates information from the entire sequence after mapping tokens into a higher-dimensional space \mathbb{R}^D through a learned polynomial function—hence the name *Polynomial Mixer*.

Figure 2. **Polynomial Mixer.** An input sequence X of n tokens with dimension d follows two parallel paths. In the top path, each token is first expanded from dimension d to D , then transformed through a polynomial of degree k with coefficients α (all multiplications and exponentiations are element-wise). Dimension k is collapsed by summation, yielding a shared state $H(X) \in \mathbb{R}^D$. In the bottom path, each token produces gating coefficients in $[0, 1]^D$, which query information from $H(X)$ via element-wise multiplication (broadcasted across n). The result is finally projected back to the original dimension d .



Formally, the sequence $X \in \mathbb{R}^{d \times n}$ is summarized into a single representation $H(X) \in \mathbb{R}^{D \times 1}$, defined as a polynomial of degree k :

$$H(X) = \left[\sum_{p=1}^k \alpha_p \odot h(W_h X)^p \right] \mathbf{1}, \quad (1)$$

where D is the internal feature dimension, $\alpha \in \mathbb{R}^{D \times k}$ are the polynomial coefficients, h is an activation function, \odot denotes the element-wise (Hadamard) product with broadcasting, and $\mathbf{1}$ is a vector of ones used to sum over the sequence dimension n . The exponentiation is also applied element-wise. The matrix $W_h \in \mathbb{R}^{D \times d}$ is a learnable parameter that mixes dimensions to ensure $H(X)$ is composed of inter-dimension polynomials instead of just monomials.

Each token then queries the shared representation $H(X)$ using the gating coefficient $S(X) = \sigma(W_s X) \in [0, 1]^{D \times n}$ and the resulting information is projected back into the original space by W_o :

$$\text{PoM}(X) = W_o [\sigma(W_s X) \odot H(X)], \quad (2)$$

where σ is the sigmoid function, and $W_o \in \mathbb{R}^{d \times D}$ and $W_s \in \mathbb{R}^{D \times d}$ are learnable parameters. All operations are linear in the sequence length n .

PolyMorpher. Drawing inspiration from Transformer architectures, we define a *PolyMorpher* block P that alternates residual Polynomial Mixer and feed-forward layers:

$$P(X) = X + \text{PoM}(X) + \text{FF}(X + \text{PoM}(X)), \quad (3)$$

where $\text{FF}(X)$ denotes a standard two-layer feed-forward network. The PolyMorpher thus acts as a *drop-in replacement* for Transformer blocks based on MHA, fulfilling the same sequence-to-sequence mapping role. The key difference lies in its parametrization: while Transformers are configured by the number of heads and their dimension, the Polymorpher is defined by the degree k and the internal dimension D of its polynomial.

3.2. Polymorpher for Causal Sequences

We consider a sequence with a causal structure encoded by a binary mask $M \in \{0, 1\}^{n \times n}$, where $M_{s,t} = 1$ if and only if token s is allowed to use information from token t to update its representation. The Polynomial Mixer can be readily adapted to handle such causal dependencies by defining a distinct state representation $H(X)$ for each time step of the sequence:

$$H(X) = \left[\sum_{p=1}^k \alpha_p \odot h(W_h X)^p \right] M^\top. \quad (4)$$

Here, $H(X) \in \mathbb{R}^{D \times n}$, and the formulation in Equation (2) remains unchanged.

Causal Sequence. In the special case of causal sequences, the mask M is a lower triangular matrix. This allows computing the state representation at time step t , denoted $H(X)_t$, through the following iterative process:

$$H(X)_t = \sum_{s \leq t} \left[\sum_{p=1}^k \alpha_p \odot h(W_h X)^p \right]_s, \quad (5)$$

$$= H(X)_{t-1} + \left[\sum_{p=1}^k \alpha_p \odot h(W_h X)^p \right]_t. \quad (6)$$

This formulation enables $\mathcal{O}(1)$ inference complexity in the autoregressive setting, a property shared with recurrent networks but not with transformers. Similar to SSMS, Polymorphers combine the advantages of both worlds: they can be trained on the entire sequence in parallel while supporting efficient recursive inference.

Block Causal Sequence. Polymorphers can also model *block-causal* sequences, as found in spatio-temporal data such as videos or satellite image time series. In this setting, each token can attend to all tokens within the same frame,

as well as to tokens from preceding frames. Let M denote a block-causal mask for a block size K :

$$M_{i,j} = 1 \text{ if } j \leq \lceil i/K \rceil K \text{ else } 0. \quad (7)$$

The state representation H can then be computed as

$$H(X)_t = H(X)_{\lfloor t/K \rfloor K} + \sum_{s=\lfloor t/K \rfloor K}^{\lceil t/K \rceil K} \left[\sum_{p=1}^k \alpha_p \odot h(W_h X)^p \right]_s. \quad (8)$$

This formulation allows processing tokens in blocks during inference, reducing memory requirements while preserving causal dependencies.

3.3. Theoretical Analysis

We first show that PoM is *equivariant*, which means that permutations in the input sequence result in permuted outputs. This is a key property that made transformers popular and does not hold for other architectures like convolutions or recurrent networks.

Proposition 3.1 (Permutation equivariance). *A Polynomial Mixer is permutation equivariant, i.e., let $X \in \mathbb{R}^{d \times n}$ be a set of vectors and P a column permutation matrix, then $PoM(XP) = PoM(X)P$.*

Proof. For a permutation P , we have

$$PoM(XP) = W_o [\sigma(W_s XP) \circ H(XP)\mathbf{1}^\top]. \quad (9)$$

We have that $H(XP) = H(X)$ because the sum is permutation invariant, and $\sigma(W_s XP) = \sigma(W_s X)P$ because σ is an element-wise operation. Noticing that $H(X)\mathbf{1}^\top$ has all identical columns allows us to move P outside of the brackets to conclude the proof. \square

More importantly, we can also prove a universal approximation theorem for Polymorphers similar to what is well known for Transformers [77]. As the polynomial mixer is equivariant, it requires the use of positional encoding (learned for simplicity reasons), which also underlines the similarity between PoM and MHA.

We use the following standard definition of distance between functions that map sequences to sequences. Given two functions f and $g : \mathbb{R}^{d_n} \rightarrow \mathbb{R}^{d_n}$ and an integer $A \leq p \leq \infty$, we define the distance d_p as:

$$d_p(f, g) = \left(\int \|f(X) - g(X)\|_p^p dX \right)^{1/p}. \quad (10)$$

The following theorem holds:

Theorem 3.2 (Universal approximation). *Let $1 \leq p \leq \infty$ and $\epsilon > 0$, then for any given $f \in \mathcal{F}$ the set of continuous functions that map a compact domain in $\mathbb{R}^{d \times n}$ to $\mathbb{R}^{d \times n}$, there exists a Polymorpher g with learned positional encoding such that $d_p(f, g) \leq \epsilon$.*

The proof follows exactly the same scheme as in [77], where most of the heavy lifting is done by the feed-forward networks. Their main argument is to show that MHA can map every token in the sequence to a unique value that depends on the entire sequence, and then the feed-forward blocks can map those unique values to the desired output. In our case, we just have to ensure that the Polynomial Mixer has the same properties as MHA, which is obtained using the following lemma:

Lemma 3.3 (Contextual mapping (informal)). *There exists $k > 0$ for which any Polynomial Mixer q of degree k is a contextual mappings on $\mathbb{R}^{d \times n}$, that is:*

- For any $X \in \mathbb{R}^{d \times n}$ with different entries, $q(X)$ has different entries.
- For any $X, X' \in \mathbb{R}^{d \times n}$ that differ at least by one element, then all entries of $q(X)$ and $q(X')$ are different.

The proof is deferred to the appendix and primarily uses the fact that a sufficiently high degree polynomial is uniquely defined by a sequence of point-wise evaluation. As noted in [77], having the contextual mapping property is not so common as it requires to summarize uniquely the context while preserving the identity of the current token.

With these results, we show that a Polymorpher is as potent as a Transformer for sequence modeling.

3.4. Complexity and Efficiency Analysis

When is PoM faster than MHA? For a sequence of length n , the cost of PoM breaks down as follows: $2dDn$ multiplications for input projections, nkD multiplications to compute the polynomial, and nD sums to aggregate it. The selection operation costs nD multiplications, and the output projection costs nDd . Assuming that the cost of additions is negligible in front of that of multiplications, this gives us a total cost of $3ndD + (k+1)nD$ multiplications.

In comparison, the cost of input projections for attention is $3nd^2$ multiplications. Then, the cost of computing the attention matrix is dn^2 multiplications and aggregating the values is also dn^2 multiplications. Finally, the output projection cost is nd^2 . This sums to a total cost of $4nd^2 + 2dn^2$.

Solving for n leads to PoM being faster when

$$n \geq \frac{D(3d+k+1) - 4d^2}{2d}, \quad (11)$$

with the polynomial degree k and the hidden dimension D setting different trade-offs. In our experiments, we found that $D = 2d$ and $k = 2$ is sufficient to match the performances of attention. In this case, PoM has a complexity advantage for $n \geq d + 3$ which usually amounts to sequences of sizes greater than 1k tokens ($d = 512-1024$).

Below this range, highly optimized attention kernels can remain competitive; however, as n grows, the cost of MHA increases quadratically while PoM grows linearly, making

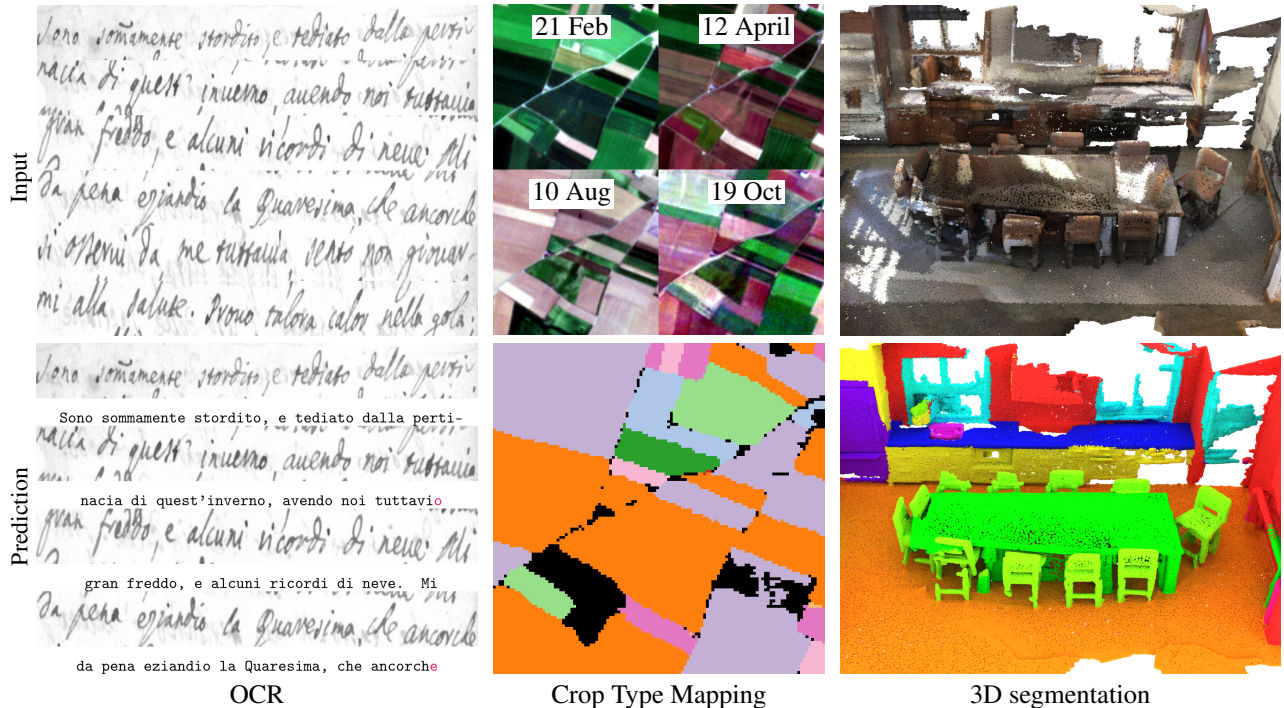


Figure 3. **Evaluation Across Domains.** We evaluate PoM on various tasks from multiple domains, simply replacing some or all the self-attention blocks in SOTA Transformer-based models. *Left:* For OCR, given a page of handwritten text (top) split into lines, the goal is to recognize each character and group them into words (bottom). *Middle:* For Earth observation, given a time series of satellite images (top), the goal is to classify each pixel as a crop type by the end of the series (bottom). *Right:* For 3D segmentation, given a 3D point cloud (top), the goal is to classify each point according to classes (bottom).

PoM significantly more efficient for long-context applications. This trend is especially pronounced in settings such as high-resolution image or video modeling, geospatial sequences, or autoregressive generation over long documents, where PoM’s linear scaling yields substantial speedups.

Comparing with Flash-Attention. Highly optimized attention implementations such as FlashAttention [18] achieve near-linear runtime for moderate sequence lengths through clever memory management and custom CUDA kernels. In contrast, our PoM implementation is written entirely in high-level PyTorch, requiring no compilation or specialized code. Despite this, PoM already demonstrates superior scalability for long sequences and large images, but remain slower for smaller ones. We argue that directly comparing new methods with highly-optimized implementations should be interpreted cautiously. This paper presents a proof of concept, showcasing PoM’s efficiency and versatility across several domains and multiple tasks. We expect further gains with dedicated low-level optimization which are out of the scope of our proof of concept.

4. Experiments

We evaluate PoM across a diverse set of tasks and modalities: natural language processing (Sec. 4.1), optical character recognition (Sec. 4.2), Earth observation analysis (Sec. 4.3), 3D point cloud segmentation (Sec. 4.4), and image generation (Sec. 4.5). Examples for the visual tasks are shown in Figure 3. This diversity highlights that PoM can serve as a drop-in, compute-efficient replacement for the standard self-attention transformer block.

We also explore the validity of hybrid models which retain some attention layers. In all our experiments, we do not introduce major architectural changes compared to the original models, but we parametrize PoM and the MLP in the blocks so as to keep the total number of parameters close to the original one. We also do not deviate from their original training recipe, except for experiments where changing the number of tokens would create training instabilities both for attention and PoM.

4.1. Natural Language Processing

Setting. We train 125M GPT-2 models on 15B tokens from FineWeb [56], following the nanoGPT setup [40]. We evaluate models using validation loss, accuracy on the fol-

Model	Val	ARC-E	HellaSwag	Winogrande	MMLU
	Loss↓	Acc.Norm↑	Acc.Norm↑	Acc.↑	Acc.↑
GPT2-S (OpenAI)	-	42.8	31.6	50.0	26.1
GPT2-S 12MHA	3.29	29.4	33.3	49.4	24.6
🍏GPPoM2-S	3.88	28.7	27.4	48.6	25.5
🍏GPPoM2-S Hyb.	3.31	29.0	33.8	51.9	25.6

(a) **Performance.** Comparison of GPT2 trained on 15B tokens from FineWeb and its GPPoM2 version.

Sequence length	1k	4k	16k	32k
GPT2-S MHA	572.3	294.6	99.3	52.4
🍏GPPoM2-S $k = 2$	995.7	893.1	624.2	447.5
$k = 3$	993.5	890.5	622.79	445.78
$k = 5$	995.6	890.2	617.10	439.51
🍏GPPoM2-S Hyb.	796.1	533.4	227.8	128.7
Mamba	56.4	56.1	56.8	56.7

(b) **Efficiency.** Token processing speed (in k-tokens/s) at which models are processing (forward) sequences of varying length.

Table 1. **Natural Language Processing.**

lowing benchmarks: ARC-E [12], HellaSwag [78], Winogrande [61], and MMLU [32]. We measure generation speed measured as the time to produce the last token in sequences of varying lengths.

We consider two configurations: (i) **GPPoM2**, where every self-attention block is replaced by a Polymorpher, and (ii) **GPPoM2 Hyb.**, where pairs of self-attention blocks are replaced by one Polymorpher and one local-attention block with a causal context limited to the last 128 tokens. This hybrid design combines the global receptive field of PoM’s state representation with the local, fine-grained modeling of attention; this is conceptually similar to how LSTMs blend long- and short-range dependencies [34]. Moreover, the hybrid architecture preserves a constant computational cost during autoregressive inference, since the local attention context is fixed.

Results. As reported in Tab. 1a, GPPoM2 achieves performance comparable, though slightly below, that of full-attention Transformers. It is worth noting that all training hyperparameters were tuned specifically for standard Transformers and we did not change the training recipe. In contrast, the Hybrid GPPoM matches, and occasionally surpasses, the performance of GPT2-S, including the checkpoint released by OpenAI that was trained on an order of magnitude more data. Both GPPoM variants are substantially more efficient than Transformers, owing to their linear-time complexity. We show in Table 1b the average speed for a forward pass on a fix token budget (from 128 batches of 1024 tokens to 4 batches of 32k tokens), using custom triton kernels. PoM-based models are even substantially faster than Mamba, which only beats attention at very long sequence lengths due to the optimization in Flash-Attention. The degree k does not have impact on the speed.

Model	#Params $\times 10^6$	Performance		Throughput	
		CER↓	WER↓	lines/s	
LAM	HTR-VT	53.5	2.8	7.4	620.2
	🍏HTR-VPoM	53.7	3.2	9.0	623.3
	🍏HTR-VPoM Hyb.	53.5	2.8	7.5	622.7
LAM-Mul	HTR-VT	54.9	3.3	9.3	598.4
	🍏HTR-VPoM	55.2	3.7	10.9	675.5
	🍏HTR-VPoM Hyb.	55.1	3.3	9.3	636.6

Table 2. **Optical Character Recognition.** We compare HTR-VT and HTR-VPoM on LAM single line and LAM multiline dataset. We report the Character Error Rate (CER), Word Error Rate (WER), and throughput (lines/s). The multiline experiments are trained for half the steps.

4.2. OCR

Setting. We assess the effectiveness of PoM on a optical character recognition task (OCR). We use the SOTA HTR-VT [45], a ViT based encoder only network, as our baseline. We conduct our experiments on the Ludovico Antonio Muratori (LAM) [7] dataset which consists of 25,823 lines in total. To showcase the benefits of PoM over standard attention we conduct two experiments, specifically, (i) Single line prediction and (ii) Multiple line prediction. Given the HTR-VT network only has four attention blocks we experiment with two type of PoM architecture: (i) HTR-VPoM: replacing all the attention layers from HTR-VT to PoM layers and (ii) HTR-VPoM Hybrid: alternating attention layers and PoM layers that perform full attention (no causal mask).

Results. We report the scores in Tab. 2. For the single-line prediction experiments, PoM based architectures are on-par with attention regarding CER (character error rate) and WER (word error rate). However, given the sequence length is just 128 tokens, attention benefits from the low occupancy level of the GPU to compensate for its quadratic cost. To take advantage of the linear cost of PoM, we also consider predicting entire pages at a time, consisting of multiple lines. We concatenate lines from the same page to produce a wide image, similar to unrolling the page horizontally. This adds up to 16 lines, or about 2k tokens on average. On this multi-line setup, the performances of HTR-VT are slightly degraded (3.3 CER vs 2.8 originally) which may come from underfitting a larger input signal. HTR-VPoM Hybrid is on par with the original architecture, while increasing throughput by about 6%. HTR-VPoM obtains 0.4 worst CER but achieves a significant 12% speedup compared to Flash-Attention. Interestingly, the throughput of PoM models is higher in the multi-line setup than in the single line setup¹, the opposite of attention models. This demonstrates the superior scalability of PoM compared to attention, even with Flash-Attention.

¹We assume this is due to the GPU being under-occupied and the latency having a bigger impact.


Model	#Params	Performance		Throughput
	$\times 10^6$	OA \uparrow	mIoU \uparrow	km ² /s
TSViT (paper)	1.7	83.4	65.1	-
TSViT (retrained)	1.7	82.8	64.6	7.2
 TSViPoM	1.7	82.7	64.6	26.3

Table 3. **Satellite Image Time Series Segmentation.** We compare of TSViT and TSViPoM on PASTIS fold 1. We report the overall accuracy (OA), mean IoU (mIoU), and throughput.

4.3. Earth Observation Analysis

Setting. We evaluate PoM on a standard geospatial task: crop type mapping from satellite multi-spectral image time series. Experiments are conducted on fold 1 of the PASTIS dataset [60], which contains Sentinel-2 time series with 10 spectral bands at a spatial resolution of 10 m per pixel. Each pixel is annotated with one of 19 crop type classes. We report overall accuracy (OA), mean Intersection over Union (mIoU), FLOPs, and throughput.

Our baseline is the TSViT model [65], a state-of-the-art architecture for supervised crop segmentation that alternates between temporal and spatial self-attention layers. We construct **TSViPoM** by replacing all Transformer blocks in TSViT with Polymorpher blocks, keeping the rest of the architecture unchanged.

Results. TSViPoM achieves performance comparable to the TSViT baseline while offering a substantial speedup—over 300% faster inference—demonstrating the efficiency of PoM as a drop-in replacement for attention in spatio-temporal modeling. This improvement is particularly relevant for geospatial applications, where inputs often span long temporal sequences, large spatial extents, and multiple spectral bands. In such settings, the quadratic scaling of self-attention becomes a major bottleneck, forcing practitioners to crop scenes, reduce temporal resolution, or downsample spectral information. By contrast, PoM’s linear complexity allows the model to process long and high-dimensional sequences directly, preserving temporal continuity and spectral richness while maintaining fast and memory-efficient inference.

4.4. Point Cloud Segmentation

Setting. We evaluate PoM for 3D point cloud semantic segmentation on two standard benchmarks: indoor scene understanding with ScanNet [14] and autonomous driving with SemanticKITTI [5]. Our baseline is the state-of-the-art PointTransformerV3 (PTv3) [74], which serializes point clouds along space-filling curves that preserve local geometric continuity. These serialized sequences are hierarchically pooled to form a U-Net-like encoder–decoder architecture. At each scale, PTv3 applies several multi-head attention (MHA) layers with a local context of 1024 points,

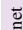





Model	#Param	Performance	Throughput	
	$\times 10^6$	mIoU \uparrow	10 ⁶ pts/s	
 ScanNet	PTv3	46.2	76.7	1.98
	 PPOmv3	47.9	75.9	2.17
	 PPOmv3 Hyb.	46.8	76.8	2.01
 SKITTI	PTv3	46.2	67.2	1.12
	 PPOmv3	47.9	66.6	1.22
	 PPOmv3 Hyb.	46.8	67.5	1.15

Table 4. **3D Point Cloud Segmentation.** We compare PTv3 with PPOmv3 on two classic 3D datasets.

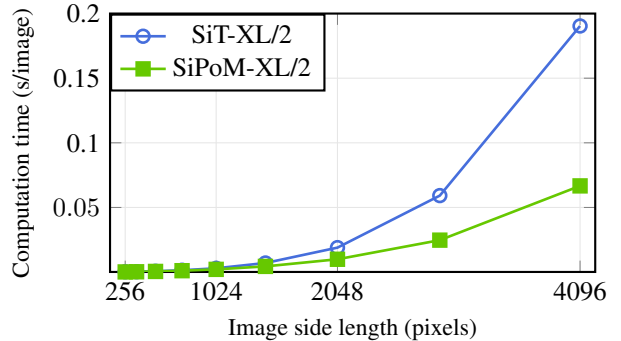


Figure 4. **Computational Efficiency.** We report the speed at generating image for various resolutions for SiT-XL/2 and its PoM counterpart SiPoM-XL/2.

a limit imposed by the quadratic cost of attention and GPU memory constraints.

We investigate two PoM-based replacements for the attention modules: (i) **PPOmv3**, which replaces all MHA layers with PoM while keeping the same context length, and (ii) **PPOmv3-Hybrid**, which alternates MHA layers, and PoM layers with a context window of 4096 points in the two highest-resolution stages of the U-Net.

Results. Results are reported in Tab. 4. The hybrid PPOmv3 matches or slightly surpasses PTv3 on both datasets while reducing computation time by 2%. Pure PoM models are up to 10% faster than Flash-Attention, with only a minor drop in accuracy. A practical advantage of PoM’s linear complexity is that entire point clouds can be processed in memory without chunking. While this does not translate into accuracy gains on standard CV benchmarks, it is a significant benefit for large-scale industrial applications where clean spatial partitioning such as single rooms is not applicable.

4.5. Class-Conditional Image Generation

Setting. We evaluate PoM on a class-conditional image generation task. For that matter, we take the popular SiT architecture [52] and replace all Attention blocks with PoM blocks. We use the AdaLNZero strategy to condition the network on the class. We consider 2 sizes of models,



Figure 5. **Qualitative Results on Class-Conditional Generation.** Images sampled from SiPoM-XL/2 with different classes at 256 resolution. We use classifier-free guidance with $\omega = 6$.

Model	#Param $\times 10^6$	Performance FID \downarrow	Throughput img/s
SiT-L/2	458	18.8	9842
🍏SiPoM-L/2	414	17.6	11,954
SiT-XL/2	675	17.2	4041
🍏SiPoM-XL/2	609	17.2	8146

Table 5. **Class-Conditional Image Generation.** We compare SiT [52] with SiPoM trained on ImageNet for generating images of resolution 256^2 for a batch size of 1024.

namely SiT-L and SiT-XL with a patch-size of 2, leading to our PoM variant named SiPoM-L/2 and SiPoM-XL/2 respectively. The training is performed on ImageNet at 256 resolution, with the same training parameters as in the original paper. The performances are evaluated with FID as is standard for this task. The efficiency is measured as throughput, which is the number of images per second that can be processed by a forward pass of the network for a batch size of 1024 images.

Quantitative results We compare the results of our SiPoM models to the original scores from [52] on Table 5. Our SiPoM variants achieve the same visual fidelity as the original attention-based models, as measured by the FID. We also measure the throughput of the SiT-XL/2 and the SiPoM-XL/2 models at various resolution, which we report in Figure 4. As expected, SiPoM becomes much more efficient than its attention-based counterpart at higher resolutions, starting at 1024 pixels per side. This is easily explain by the number of tokens growing quadratically with the resolution of the images, leading to longer sequences which further accentuate the gap between linear cost of PoM and

the quadratic cost of attention.

Qualitative results We show images sampled from SiPoM-XL/2 in Figure 5. The images are sampled using Classifier Free Guidance with $\omega = 6$. The visual quality of the images is on par with equivalent models from the literature. This validates that SiPoM-XL/2 is able to produce the same quality of pictures as its attention counterpart.

5. Conclusion

We introduced **PoM**, the *Polynomial Mixer*, a neural network building block that serves as a drop-in, efficient replacement for self-attention in Transformer architectures. PoM combines *linear complexity* with the *universal sequence-to-sequence approximator*. We validated PoM across five diverse domains—natural language processing, Earth observation, 3D point cloud segmentation, optical character recognition, and image generation. We demonstrate that hybrid PoM/self-attention architectures consistently match or surpass the performance of full-attention models while offering superior speed and scalability.

These properties make PoM a compelling choice for long-sequence applications such as high-definition video generation or multimodal large language models, which could greatly benefit from its $\mathcal{O}(1)$ inference under causal masking. While large-scale experiments remain beyond our current computational scope, PoM lays the groundwork for the next generation of efficient, general-purpose, attention-free sequence models.

6. Acknowledgment

This work was supported by ANR project sharp ANR-23-PEIA-0008 in the context of the PEPR IA. This project was provided with computing and storage resources by GENCI at IDRIS thanks to the grants 2025-A0191013085 and 2025-A0181016234 on the supercomputer Jean Zay’s H100 partition. The authors would like to thank Vincent Lepetit, Gül Varol and Dimitris Samaras for their insightful comments and suggestions.

References

- [1] Josh Achiam, Steven Adler, Sandhini Agarwal, Lama Ahmad, Ilge Akkaya, Florencia Leoni Aleman, Diogo Almeida, Janko Altmenschmidt, Sam Altman, Shyamal Anadkat, et al. GPT-4 technical report. *arXiv:2303.08774*, 2023.
- [2] Alexei Baevski, Yuhao Zhou, Abdelrahman Mohamed, and Michael Auli. wav2vec 2.0: A framework for self-supervised learning of speech representations. *NeurIPS*, 2020.
- [3] Xingjian Bai and Luke Melas-Kyriazi. Fixed point diffusion models. In *CVPR*, 2024.
- [4] Yogesh Balaji, Seungjun Nah, Xun Huang, Arash Vahdat, Jiaming Song, Qingsheng Zhang, Karsten Kreis, Miika Aittala, Timo Aila, Samuli Laine, Bryan Catanzaro, Tero Karras, and Ming-Yu Liu. eDiff-I: Text-to-image diffusion models with ensemble of expert denoisers. *arXiv:2211.01324*, 2022.
- [5] Jens Behley, Martin Garbade, Andres Milioto, Jan Quenzel, Sven Behnke, Cyrill Stachniss, and Jurgen Gall. SemanticKITTI: A dataset for semantic scene understanding of LiDAR sequences. In *ICCV*, 2019.
- [6] William Brandon, Mayank Mishra, Aniruddha Nrusimha, Rameswar Panda, and Jonathan Ragan Kelly. Reducing transformer key-value cache size with cross-layer attention. *NeurIPS*, 2024.
- [7] Silvia Cascianelli, Vittorio Pippi, Martin Maarand, Marcella Cornia, Lorenzo Baraldi, Christopher Kermorvant, and Rita Cucchiara. The LAM dataset: A novel benchmark for line-level handwritten text recognition. In *ICPR*, 2022.
- [8] Junsong Chen, Chongjian Ge, Enze Xie, Yue Wu, Lewei Yao, Xiaoze Ren, Zhongdao Wang, Ping Luo, Huchuan Lu, and Zhenguo Li. Pixart- σ : Weak-to-strong training of diffusion transformer for 4k text-to-image generation. In *ECCV*, 2024.
- [9] Ting Chen and Lala Li. FIT: Far-reaching interleaved transformers. *arXiv:2305.12689*, 2023.
- [10] Rewon Child, Scott Gray, Alec Radford, and Ilya Sutskever. Generating long sequences with sparse transformers. *arXiv:1904.10509*, 2019.
- [11] Chung-Cheng Chiu, James Qin, Yu Zhang, Jiahui Yu, and Yonghui Wu. Self-supervised learning with random-projection quantizer for speech recognition. In *International Conference on Machine Learning*. PMLR, 2022.
- [12] Peter Clark, Isaac Cowhey, Oren Etzioni, Tushar Khot, Ashish Sabharwal, Carissa Schoenick, and Oyvind Tafjord. Think you have solved question answering? Try ARC, the AI2 reasoning challenge. *arXiv:1803.05457*, 2018.
- [13] Katherine Crowson, Stefan Andreas Baumann, Alex Birch, Tanishq Mathew Abraham, Daniel Z Kaplan, and Enrico Shippole. Scalable high-resolution pixel-space image synthesis with hourglass diffusion transformers. In *Int. Conf. Mach. Learn.*, 2024.
- [14] Angela Dai, Angel X. Chang, Manolis Savva, Maciej Halber, Thomas Funkhouser, and Matthias Niessner. ScanNet: Richly-annotated 3D reconstructions of indoor scenes. In *CVPR*, 2017.
- [15] Tri Dao. FlashAttention-2: Faster attention with better parallelism and work partitioning. *ICLR*, 2024.
- [16] Tri Dao and Albert Gu. Transformers are SSMs: Generalized models and efficient algorithms through structured state space duality. In *Int. Conf. Mach. Learn.*, 2024.
- [17] Tri Dao, Dan Fu, Stefan Ermon, Atri Rudra, and Christopher Ré. FlashAttention: Fast and memory-efficient exact attention with io-awareness. In *NeurIPS*, 2022.
- [18] Tri Dao, Daniel Y. Fu, Stefano Ermon, Atri Rudra, and Christopher Ré. FlashAttention: Fast and memory-efficient exact attention with IO-awareness. In *NeurIPS*, 2022.
- [19] Alexandre Défossez, Laurent Mazaré, Manu Orsini, Amélie Royer, Patrick Pérez, Hervé Jégou, Edouard Grave, and Neil Zeghidour. Moshi: A speech-text foundation model for real-time dialogue. *arXiv:2410.00037*, 2024.
- [20] Alexey Dosovitskiy, Lucas Beyer, Alexander Kolesnikov, Dirk Weissenborn, Xiaohua Zhai, Thomas Unterthiner, Mostafa Dehghani, Matthias Minderer, Georg Heigold, Sylvain Gelly, et al. An image is worth 16x16 words: Transformers for image recognition at scale. In *ICLR*, 2020.
- [21] Abhimanyu Dubey, Abhinav Jauhri, Abhinav Pandey, Abhishek Kadian, Ahmad Al-Dahle, Aiesha Letman, Akhil Mathur, Alan Schelten, Amy Yang, Angela Fan, et al. The LLAMA 3 herd of models. *arXiv:2407.21783*, 2024.
- [22] Nicolas Dufour, Victor Besnier, Vicky Kalogeiton, and David Picard. Don’t drop your samples! Coherence-aware training benefits conditional diffusion. In *CVPR*, 2024.
- [23] Patrick Esser, Sumith Kulal, Andreas Blattmann, Rahim Entezari, Jonas Müller, Harry Saini, Yam Levi, Dominik Lorenz, Axel Sauer, Frederic Boesel, et al. Scaling rectified flow transformers for high-resolution image synthesis. In *Int. Conf. Mach. Learn.*, 2024.
- [24] Peng Gao, Le Zhuo, Ziyi Lin, Chris Liu, Junsong Chen, Ruoyi Du, Enze Xie, Xu Luo, Longtian Qiu, Yuhang Zhang, et al. Lumina-T2X: Transforming text into any modality, resolution, and duration via flow-based large diffusion transformers. *arXiv:2405.05945*, 2024.
- [25] Paolo Gloriosio, Quentin Anthony, Yury Tokpanov, James Whittington, Jonathan Pilault, Adam Ibrahim, and Beren Millidge. Zamba: A compact 7B SSM hybrid model. *arXiv:2405.16712*, 2024.
- [26] Aaron Gokaslan, A. Feder Cooper, Jasmine Collins, Landon Seguin, Austin Jacobson, Mihir Patel, Jonathan Frankle, Cory Stephenson, and Volodymyr Kuleshov. CommonCanvas: Open diffusion models trained on creative-commons images. In *CVPR*, 2024.
- [27] Albert Gu, Karan Goel, and Christopher Re. Efficiently modeling long sequences with structured state spaces. In *ICLR*, 2021.

- [28] Albert Gu, Isys Johnson, Karan Goel, Khaled Saab, Tri Dao, Atri Rudra, and Christopher Ré. Combining recurrent, convolutional, and continuous-time models with linear state space layers. In *NeurIPS*, 2021.
- [29] Jiatao Gu, Shuangfei Zhai, Yizhe Zhang, Joshua M Susskind, and Navdeep Jaitly. Matryoshka diffusion models. In *ICLR*, 2023.
- [30] Tiankai Hang and Shuyang Gu. Improved noise schedule for diffusion training. *ICCV*, 2024.
- [31] Ali Hatamizadeh, Jiaming Song, Guilin Liu, Jan Kautz, and Arash Vahdat. DiffFit: Diffusion vision transformers for image generation. In *ECCV*, 2024.
- [32] Dan Hendrycks, Collin Burns, Steven Basart, Andy Zou, Mantas Mazeika, Dawn Song, and Jacob Steinhardt. Measuring massive multitask language understanding. In *ICLR*, 2021.
- [33] Jonathan Ho, Ajay Jain, and Pieter Abbeel. Denoising diffusion probabilistic models. In *NeurIPS*, 2020.
- [34] Sepp Hochreiter and Jürgen Schmidhuber. Long short-term memory. *Neural computation*, 1997.
- [35] Vincent Tao Hu, Stefan Andreas Baumann, Ming Gui, Olga Grebenkova, Pingchuan Ma, Johannes Fischer, and Björn Ommer. ZigMa: A DiT-style zigzag Mamba diffusion model. In *ECCV*, 2024.
- [36] Allan Jabri, David J Fleet, and Ting Chen. Scalable adaptive computation for iterative generation. In *Int. Conf. Mach. Learn.*, 2023.
- [37] Pierre Jacob, David Picard, Aymeric Histace, and Edouard Klein. Metric learning with horde: High-order regularizer for deep embeddings. In *ICCV*, pages 6539–6548, 2019.
- [38] Andrew Jaegle, Sebastian Borgeaud, Jean-Baptiste Alayrac, Carl Doersch, Catalin Ionescu, David Ding, Skanda Koppula, Daniel Zoran, Andrew Brock, Evan Shelhamer, et al. Perceiver IO: A general architecture for structured inputs & outputs. In *ICLR*, 2022.
- [39] Jared Kaplan, Sam McCandlish, Tom Henighan, Tom B Brown, Benjamin Chess, Rewon Child, Scott Gray, Alec Radford, Jeffrey Wu, and Dario Amodei. Scaling laws for neural language models. *arXiv preprint arXiv:2001.08361*, 2020.
- [40] Andrej Karpathy. NanoGPT. <https://github.com/karpathy/nanoGPT>, 2022.
- [41] Tero Karras, Miika Aittala, Jaakko Lehtinen, Janne Hellsten, Timo Aila, and Samuli Laine. Analyzing and improving the training dynamics of diffusion models. In *CVPR*, 2024.
- [42] Tero Karras, Miika Aittala, Jaakko Lehtinen, Janne Hellsten, Timo Aila, and Samuli Laine. Analyzing and improving the training dynamics of diffusion models. In *CVPR*, 2024.
- [43] Nikita Kitaev, Lukasz Kaiser, and Anselm Levskaya. ReFormer: The efficient transformer. In *ICLR*, 2020.
- [44] Seung Hyun Lee, Yinxiao Li, Junjie Ke, Innfarn Yoo, Han Zhang, Jiahui Yu, Qifei Wang, Fei Deng, Glenn Entis, Junfeng He, et al. Parrot: Pareto-optimal multi-reward reinforcement learning framework for text-to-image generation. In *ECCV*, 2025.
- [45] Yuting Li, Dexiong Chen, Tinglong Tang, and Xi Shen. HTR-VT: Handwritten text recognition with vision transformer. *Pattern Recognition*, 2025.
- [46] Opher Lieber, Barak Lenz, Hofit Bata, Gal Cohen, Jhonathan Osin, Itay Dalmedigos, Erez Safahi, Shaked Meir, Yonatan Belinkov, Shai Shalev-Shwartz, et al. Jamba: A hybrid transformer-Mamba language model. *ICLR*, 2025.
- [47] Yaron Lipman, Ricky TQ Chen, Heli Ben-Hamu, Maximilian Nickel, and Matthew Le. Flow matching for generative modeling. In *ICLR*, 2022.
- [48] Xingchao Liu, Chengyue Gong, et al. Flow straight and fast: Learning to generate and transfer data with rectified flow. In *ICLR*, 2023.
- [49] Yue Liu, Yunjie Tian, Yuzhong Zhao, Hongtian Yu, Lingxi Xie, Yaowei Wang, Qixiang Ye, and Yunfan Liu. Vmamba: Visual state space model, 2024.
- [50] Yujian Liu, Yang Zhang, Tommi Jaakkola, and Shiyu Chang. Correcting diffusion generation through resampling. In *CVPR*, 2024.
- [51] Shi Luohe, Zhang Hongyi, Yao Yao, Li Zuchao, and Zhao Hai. Keep the cost down: A review on methods to optimize LLM’s KV-cache consumption. *COLM*, 2024.
- [52] Nanye Ma, Mark Goldstein, Michael S Albergo, Nicholas M Boffi, Eric Vanden-Eijnden, and Saining Xie. SIT: Exploring flow and diffusion-based generative models with scalable interpolant transformers. In *ECCV*, 2024.
- [53] Alexander Quinn Nichol and Prafulla Dhariwal. Improved denoising diffusion probabilistic models. In *Int. Conf. Mach. Learn.*, 2021.
- [54] William Peebles and Saining Xie. Scalable diffusion models with transformers. In *ICCV*, 2023.
- [55] Xiaohuan Pei, Tao Huang, and Chang Xu. EfficientV-Mamba: Atrous selective scan for light weight visual mamba, 2025.
- [56] Guilherme Penedo, Hynek Kydliček, Anton Lozhkov, Margaret Mitchell, Colin A Raffel, Leandro Von Werra, Thomas Wolf, et al. The fineweb datasets: Decanting the web for the finest text data at scale. *NeurIPS*, 2024.
- [57] David Picard and Philippe-Henri Gosselin. Improving image similarity with vectors of locally aggregated tensors. In *ICIP*, pages 669–672, 2011.
- [58] Alec Radford, Jeffrey Wu, Rewon Child, David Luan, Dario Amodei, Ilya Sutskever, et al. Language models are unsupervised multitask learners. *OpenAI blog*, 2019.
- [59] Robin Rombach, Andreas Blattmann, Dominik Lorenz, Patrick Esser, and Björn Ommer. High-resolution image synthesis with latent diffusion models. In *CVPR*, 2022.
- [60] Vivien Sainte Fare Garnot and Loic Landrieu. Panoptic segmentation of satellite image time series with convolutional temporal attention networks. *ICCV*, 2021.
- [61] Keisuke Sakaguchi, Ronan Le Bras, Chandra Bhagavatula, and Yejin Choi. Winogrande: An adversarial winograd schema challenge at scale. *Communications of the ACM*, 2021.
- [62] Yuyang Shi, Valentin De Bortoli, Andrew Campbell, and Arnaud Doucet. Diffusion Schrödinger bridge matching. In *NeurIPS*, 2024.
- [63] Chenyang Si, Ziqi Huang, Yuming Jiang, and Ziwei Liu. FreeU: Free lunch in diffusion U-net. In *CVPR*, 2024.

- [64] Yang Song, Jascha Sohl-Dickstein, Diederik P Kingma, Abhishek Kumar, Stefano Ermon, and Ben Poole. Score-based generative modeling through stochastic differential equations. In *ICLR*, 2021.
- [65] Michail Tarasiou, Erik Chavez, and Stefanos Zafeiriou. ViTs for SITS: Vision transformers for satellite image time series. In *CVPR*, 2023.
- [66] Gemini Team, Rohan Anil, Sebastian Borgeaud, Jean-Baptiste Alayrac, Jiahui Yu, Radu Soricut, Johan Schalkwyk, Andrew M Dai, Anja Hauth, Katie Millican, et al. GEMINI: A family of highly capable multimodal models. *arXiv:2312.11805*, 2023.
- [67] Gemma Team, Morgane Riviere, Shreya Pathak, Pier Giuseppe Sessa, Cassidy Hardin, Surya Bhupatiraju, Léonard Hussenot, Thomas Mesnard, Bobak Shahriari, Alexandre Ramé, et al. Gemma 2: Improving open language models at a practical size. *arXiv:2408.00118*, 2024.
- [68] Ilya O Tolstikhin, Neil Houlsby, Alexander Kolesnikov, Lucas Beyer, Xiaohua Zhai, Thomas Unterthiner, Jessica Yung, Andreas Steiner, Daniel Keysers, Jakob Uszkoreit, et al. MLP-Mixer: An all-MLP architecture for vision. In *NeurIPS*, 2021.
- [69] Hugo Touvron, Piotr Bojanowski, Mathilde Caron, Matthieu Cord, Alaaeldin El-Nouby, Edouard Grave, Gautier Izacard, Armand Joulin, Gabriel Synnaeve, Jakob Verbeek, et al. ResMLP: Feedforward networks for image classification with data-efficient training. *IEEE TPAMI*, 2022.
- [70] Ashish Vaswani, Noam Shazeer, Niki Parmar, Jakob Uszkoreit, Llion Jones, Aidan N Gomez, Łukasz Kaiser, and Illia Polosukhin. Attention is all you need. In *NeurIPS*, 2017.
- [71] Bram Wallace, Meihua Dang, Rafael Rafailov, Linqi Zhou, Aaron Lou, Senthil Purushwalkam, Stefano Ermon, Caiming Xiong, Shafiq Joty, and Nikhil Naik. Diffusion model alignment using direct preference optimization. In *CVPR*, 2024.
- [72] Sinong Wang, Belinda Z Li, Madian Khabsa, Han Fang, and Hao Ma. LinFormer: Self-attention with linear complexity. *arXiv:2006.04768*, 2020.
- [73] Fanyue Wei, Wei Zeng, Zhenyang Li, Dawei Yin, Lixin Duan, and Wen Li. Powerful and flexible: Personalized text-to-image generation via reinforcement learning. In *ECCV*, 2024.
- [74] Xiaoyang Wu, Li Jiang, Peng-Shuai Wang, Zhijian Liu, Xihui Liu, Yu Qiao, Wanli Ouyang, Tong He, and Hengshuang Zhao. Point Transformer v3: Simpler, faster, stronger. In *CVPR*, 2024.
- [75] Jing Nathan Yan, Jiatao Gu, and Alexander M Rush. Diffusion models without attention. In *CVPR*, 2024.
- [76] Zhuoyi Yang, Jiayan Teng, Wendi Zheng, Ming Ding, Shiyu Huang, Jiazheng Xu, Yuanming Yang, Wenyi Hong, Xiaohan Zhang, Guanyu Feng, et al. CogVideoX: Text-to-video diffusion models with an expert transformer. *ICLR*, 2025.
- [77] Chulhee Yun, Srinadh Bhojanapalli, Ankit Singh Rawat, Sashank Reddi, and Sanjiv Kumar. Are transformers universal approximators of sequence-to-sequence functions? In *ICLR*, 2020.
- [78] Rowan Zellers, Ari Holtzman, Yonatan Bisk, Ali Farhadi, and Yejin Choi. HellaSwag: Can a machine really finish your sentence? *arXiv:1905.07830*, 2019.
- [79] Xiaohua Zhai, Alexander Kolesnikov, Neil Houlsby, and Lucas Beyer. Scaling vision transformers. In *CVPR*, 2022.
- [80] Yu Zhang, Wei Han, James Qin, Yongqiang Wang, Ankur Bapna, Zhehuai Chen, Nanxin Chen, Bo Li, Vera Axelrod, Gary Wang, et al. Google USM: Scaling automatic speech recognition beyond 100 languages. *arXiv:2303.01037*, 2023.
- [81] Yang Zhao, Yanwu Xu, Zhisheng Xiao, Haolin Jia, and Tingbo Hou. MobileDiffusion: Instant text-to-image generation on mobile devices. In *ECCV*, 2024.
- [82] Zhenyu Zhou, Defang Chen, Can Wang, and Chun Chen. Fast ode-based sampling for diffusion models in around 5 steps. In *CVPR*, 2024.
- [83] Lianghai Zhu, Bencheng Liao, Qian Zhang, Xinlong Wang, Wenyu Liu, and Xinggang Wang. Vision Mamba: Efficient visual representation learning with bidirectional state space model. *arXiv:2401.09417*, 2024.
- [84] Jingwei Zuo, Maksim Velikanov, Dhia Eddine Rhaiem, Ilyas Chahed, Younes Belkada, Guillaume Kunsch, and Hakim Hacid. Falcon Mamba: The first competitive attention-free 7B language model. *arXiv:2410.05355*, 2024.

PoM: A Linear-Time Replacement for Attention with the Polynomial Mixer

Supplementary Material

Table 6. **Additional ablations and baselines.** MHA throughput uses Flash-Attention, Performer uses `torch_geometric`.

	ARC-easy Acc.Norm↑	HellaSwag Acc.Norm↑	Winogrande Acc.↑	Throughput 4096 tok., tok/s↑
PoM-hyb k=2	29.0	33.8	51.9	163
PoM-hyb k=3	29.5	33.4	49.6	161
PoM-hyb k=5	28.6	33.9	49.5	153
MHA	29.4	33.3	49.4	42
Performer		training failed		59
Mamba	29.3	30.8	48.0	384

In this appendix, we report additional ablations (Sec. A) and analysis (Sec. B), and a proof of our main theoretical results (Sec. C). We also propose an extended related work in depth (Sec. D) and additional illustrations for the image generation experiment (Sec. E.)

A. Additional Ablations.

Higher Orders k . We study the effect of increasing the polynomial degree k in Tab. 6. Higher-order polynomials provide a modest improvement, at the cost of a slight speed reduction. The limited impact is expected, as the sequences evaluated in classic benchmarks are relatively short and do not fully stress the model’s representational capacity. As suggested by our theoretical analysis, higher-order interactions could become more critical for distinguishing longer sequences.

Additional Baselines. We evaluate competing linear attention models and report their performance in Tab. 6.

- *Performer.* We attempted to train a GPT2-S model using Performer; however, both `pytorch-performer` and the Performer implementation from `torch_geometric` systematically diverged, producing NaN losses after a few iterations. At present, we are not aware of a well-maintained Performer implementation suitable for large-scale language model training, which prevented a fair comparison.
- *Mamba.* We trained a Mamba model of comparable size (124M parameters) on the NLP task; results are reported in Tab. 6. As expected, Mamba achieves excellent speed due to its $\mathcal{O}(1)$ complexity and dedicated CUDA kernel. PoM shares the same $\mathcal{O}(1)$ theoretical complexity, and we therefore expect that a dedicated CUDA implementation would yield comparable speedups. In terms of accuracy, however, **Mamba performs below MHA and PoM** on the evaluated benchmarks. We used the same classic training recipe inherited from attention-based models for all methods, which suggests that Mamba may require more tuning adaptation than PoM. We also observed

that **Mamba consumed approximately $4\times$ more memory** during training, forcing smaller batch sizes and gradient accumulation, whereas PoM and MHA have a similar memory footprint.

B. Additional Analysis.

Comparison to FlashAttention. FlashAttention is a highly engineered implementation of attention, relying on custom CUDA kernels and carefully optimized memory management. In contrast, PoM is currently implemented entirely in high-level PyTorch, and yet already achieves consistent $2\text{--}4\times$ speedups across tasks, and in some settings (notably NLP, see Tab. 6, and image generation), PoM is faster than Flash-Attention. We therefore view these results as a conservative estimate of PoM’s speed, and expect further gains with dedicated low-level optimization.

Generalization Under Train–Test Length Mismatch. Since $H(x)$ is obtained by pooling over tokens, its dimensionality is independent of the sequence length. In our NLP experiments, PoM is trained with a fixed sequence length of 2048 tokens (with padding), while evaluation on HellaSwag involves sequences ranging from 48 to 742 tokens, with no observable impact on performance.

C. Proof of Lemma 3

We first need to show that set with different entries are mapped to different vectors. We first separate PoM into its two components:

$$s(X) = \sigma(W_s X) \quad (12)$$

$$H(X) = \left[\sum_{p=1}^k \alpha_p \odot h(W_h X)^p \right] \mathbf{1} \quad (13)$$

$$\text{PoM}(X) = W_o [\sigma(W_s X) \odot H(X)] \quad (14)$$

Assuming $\ker(W_o) = \emptyset$, and noting that $H_k(X)$ is the same for every column, we just have to show that $s(X)$ has different columns. This is easily achieved by having $\ker(W_s) = \emptyset$ since σ is injective and the composition of injective functions is itself injective.

Second, we have to show that sets that differ by at least one element are mapped to all different entries. To simplify notations, we will consider the special case where all matrices are the identity or an identity block positioned such as to perform submatrix selection. All the matrices can thus be removed from the formula. A similar argument can be

made for matrices that are full rank as they preserve injectivity. We will also consider linear activations everywhere, which can be made as close as one wish by partitioning the image of the activation function and performing piecewise linear approximation.

With this simplified version of PoM, we have to show that for 2 sets X, X' differing by at least one element (i.e., $\exists x' \in X', \forall x \in X, x \neq x'$), then there exist k such that

$$\forall x \in X, x' \in X', x \sum_{x_i \in X} x_i^k \neq x' \sum_{x_i \in X} x_i^k. \quad (15)$$

Consider the functions $P(t)$ and $P'(t)$ defined as follows:

$$P(t) = \sum_{x_i \in X} x_i^t \quad (16)$$

$$P'(t) = \sum_{x_i \in X'} x_i^t \quad (17)$$

Since X and X' differ by at least one element, there exists at least one $x_i \in X$ such that $x_i \neq x'_i, \forall x'_i \in X'$. This implies that the functions $P(t)$ and $P'(t)$ are not identical since are sums of exponentials with different bases.

Since $P(t)$ and $P'(t)$ are different functions, there must exist some k for which $P(k) \neq P'(k)$. In other words, there exists a k such that:

$$\sum_{x_i \in X} x_i^k \neq \sum_{x'_i \in X'} x'_i{}^k \quad (18)$$

For this k , let us denote $S_k = \sum_{x_i \in X} x_i^k$. We need to show that $xS_k \neq x'S'_k$ for all $x \in X$ and $x' \in X'$. Assume for the sake of contradiction that there exist $x \in X$ and $x' \in X'$ such that $xS_k = x'S'_k$. This implies:

$$x \sum_{x_i \in X} x_i^k = x' \sum_{x'_i \in X'} x'_i{}^k \quad (19)$$

Rearranging, we get:

$$\frac{x}{x'} = \frac{\sum_{x'_i \in X'} x'_i{}^k}{\sum_{x_i \in X} x_i^k} \quad (20)$$

Since $S_k \neq S'_k$, the right-hand side is not equal to 1. However, for this equality to hold for all $x \in X$ and $x' \in X'$, the ratio x/x' would need to be constant for all pairs (x, x') , which is not possible given that X and X' differ by at least one element.

Therefore, there exists a k such that $xS_k \neq x'S'_k$ for all $x \in X$ and $x' \in X'$.

D. Related work on Diffusion

Diffusion Diffusion models [33, 53, 64] learn a neural operator that produces natural images from noise using a forward-reverse set of processes. The forward process consists in pushing the distribution of natural images forward to a known distribution, typically Gaussian, which can be done by adding increasing level of noise to the image. The reverse process does not have an explicit solution, but can be approximated by a neural network by regressing the local inverse of the forward process, i.e., solving

$$\min_{\theta} \mathbb{E}_{t \sim \mathcal{U}(0,1)} [\|\varepsilon_t - f_{\theta}(x_t, t)\|^2], \quad (21)$$

$$\text{s.t. } x_t = \alpha_t x_0 + \gamma_t \varepsilon_t, \varepsilon_t \sim \mathcal{N}(0, 1). \quad (22)$$

Here, α_t and γ_t are chosen such that x_0 corresponds to a natural image whereas x_1 corresponds to pure Gaussian noise. A great amount of research has been put into finding better noise schedules (α_t and γ_t) [4, 30, 42], or improving the quantity that is regressed [47, 48, 62], keeping the general idea of learning to invert step by step the stochastic differential equation that transforms an image into noise.

For image and generation, most efforts have been poured into designing efficient architectures at the task. While the original DDPM papers [33, 53] sample images in pixel space, making it unsuitable for large resolution, the most groundbreaking improvement was introduced by Stable Diffusion [59] with the addition of a variational auto-encoder (VAE) that allows the diffusion process to be performed in a lower dimensional latent space. Stable Diffusion uses a U-Net architecture complemented by attention layers [59, 63]. To benefit more from the scaling properties of transformers [39, 79], simpler approaches based solely on transformer layers has been proposed in DiT [54] and the subsequent flow-matching version SiT [52]. Most modern text-to-image generation models are now based on Transformer layers rather than the U-Net [8, 23, 24, 31]. [13, 29], train efficient pixel space transformers models by leveraging multiscale training and SwinAttention. Similarly, RIN [9, 36] also proposes an approach using attention only, albeit in a Perceiver-IO [38] inspired architecture that uses cross-attention to perform most of the computation in a smaller latent space, and has been successfully extended to text-to-image [22]. In addition to architectures and sampling [3, 81, 82], the importance of training is also highlighted in recent works, from resampling the training data [26, 50] to RL [44, 71, 73] and model averaging [41].

E. Uncurated Image Samples

To show 🍏PoM versatility, with train a DiPoM-XL/2 with the diffusion loss instead of the flow-matching loss and show generated samples with CFG $\omega = 6$ in the following pages.



Figure 6. Uncurated 256^2 images for the class *loggerhead*, *loggerhead turtle*, *Caretta caretta* (33).



Figure 7. Uncurated 256^2 images for the class *macaw* (88).

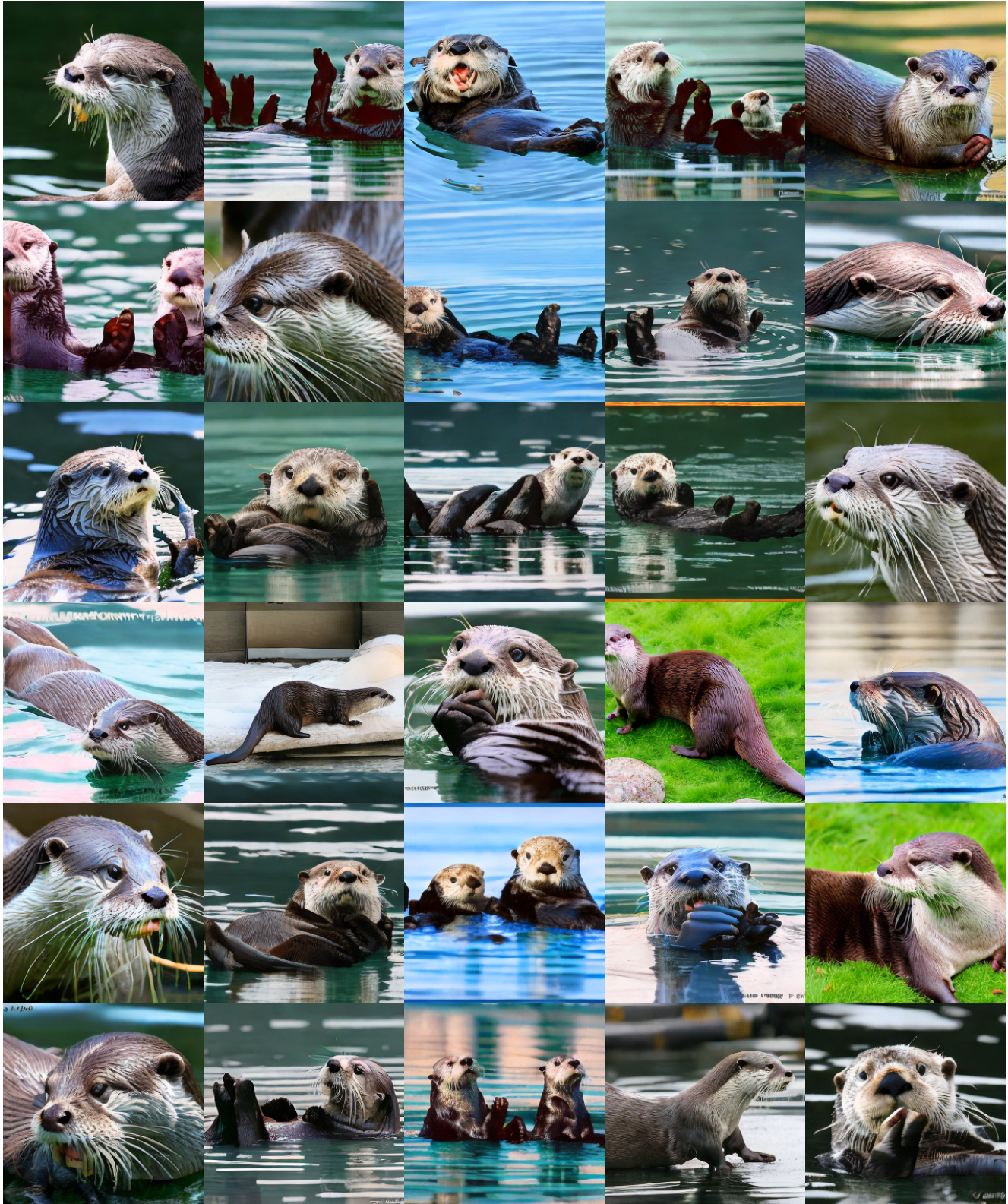


Figure 8. Uncurated 256^2 images for the class *otter* (360).



Figure 9. Uncurated 256^2 images for the class *volcano* (980).